chemistry of ligand spheres. We have observed that in aqueous solutions reduction of V(V) occurs at different rates in the presence of a number of bioligands, including citrates or α-amino acids. An excess of peroxides stabilizes V(V) in these solutions, and the redox process, which is sometimes reversible, can often be followed by the color change. In the biochemistry of vanadium, the V(V) peroxo heteroligand spheres are very likely involved as intermediates in chain reactions, undergoing ligand rearrangements with or without an electron transfer, governed by complex equilibria, and possibly radical interactions of short-lived intermediates, proposed to proceed in the catalytic processes involving V(V) peroxo complexes.[32,34,37]

In the environment of a living cell mono- rather than diperoxo(heteroligand)vanadates(V) are expected to exist because they form easily at a low or moderate hydrogen peroxide concentration. The monoperoxo complexes also proved to be more efficient catalysts.[28,32-34] Unusual and interesting rearrangement of bipyridyl[36] and substitution of nicotinic acid[37] have also been observed in monoperoxovanadates(V). Triperoxovanadates are very rare, are unstable, and exist only in alkaline media with a large excess of peroxides.[38]

Vanadium citrato complexes are of interest from yet another point of view, regarding the interaction of vanadium with transferrin. Citrato ligands are supposed to compete in the cell with transferrin for the iron and aluminum ions,[3] which form stable complexes with citrates. Experiments have shown that vanadium binds to transferrin,[14,15a,39,40] an iron-transfer protein, which may also transport vanadium.[41] Analogous ligand competition between citrates and transferrin proposed for iron may well operate for vanadium, and the character of the vanadium–citrato bond is of great interest in this respect.

Only a few stable and well-characterized monoperoxovanadates(V) are known,[11,28,36,37,42] and the oxo peroxo citrato complexes described here are an intriguing addition to the existing set of these compounds.

Acknowledgment. Support of this work by the NSF (Grants CHE-8521376 and CHE-8300516) is gratefully acknowledged.

Registry No. **1**, 118495-35-5; **2**, 118574-46-2; **3**, 118574-47-3; **4**, 118495-36-6.

Supplementary Material Available: A listing of thermal parameters (1 page); a table of calculated and observed structure factors (11 pages). Ordering information is given on any current masthead page.

(37) Puryear, B. C.; Abelt, C. J.; Djordjevic, C. *Inorg. Chim. Acta* **1988**, *149*, 15.
(38) Chaudhuri, M. K.; Ghosh, S. K. *Inorg. Chem.* **1982**, *21*, 4020.
(39) Bertini, I.; Luchinat, C.; Messori, L. *J. Inorg. Biochem.* **1985**, *25*, 57.
(40) Harris, W. R.; Carrano, C. J. *J. Inorg. Biochem.* **1984**, *22*, 201.
(41) Harris, R. W.; Friedman, S. B.; Silberman, D. *J. Inorg. Biochem.* **1984**, *20*, 157.
(42) Stomberg, R. *Acta Chem. Scand., Ser. A* **1986**, *A40*, 168.

Contribution from the Department of Chemistry, State University of New York at Albany, Albany, New York 12222

Synthesis and Chemical Characterization of Complexes Containing Semiquinone Units Bridged by Pentaoxodimolybdate Groups. Structural and Electrochemical Studies of $[(n\text{-}C_4H_9)_4N]_2[Mo_4O_{10}(C_6H_2O_4)_2]$ and $[(n\text{-}C_4H_9)_4N]_3[Mo_6O_{15}(C_6O_6)_2]$ and of an Analogous Tetraoxydibenzofuran Complex, $[(n\text{-}C_4H_9)_4N]_2[Mo_4O_{10}(C_{12}H_4O_5)_2]$, Prepared from Metal-Mediated Radical Coupling of 1,2,4-Trihydroxybenzene Precursors

Shuncheng Liu, Shahid N. Shaikh, and Jon Zubieta*

Received August 24, 1988

Reaction of $(Bu_4N)_2[Mo_2O_7]$ with 2,5-dihydroxybenzoquinone in acetonitrile yields $(Bu_4N)_2[Mo_4O_{10}(C_6H_2O_4)_2]$ (I), a tetranuclear complex with two $[Mo_2O_5]^{2+}$ units bridging two planar $(C_6H_2O_4)^{n-}$ groups, stacked in a parallel staggered orientation. The most significant feature is the short interplanar distance between ligands of 2.67 Å, allowing magnetic coupling of the radical anion semiquinoid-type ligands. Reactions of organic solvent soluble polyoxomolybdates with tetrahydroxybenzoquinone and 1,2,4-trihydroxybenzene yield the structurally analogous complexes $(Bu_4N)_3[Mo_6O_{15}(C_6O_6)_2]$ (III) and $(Bu_4N)_2[Mo_4O_{10}(C_{12}H_4O_5)_2]$ (IV). In contrast to I and IV, III is paramagnetic with an EPR spectrum consistent with electron localization in a ligand-centered orbital. The steric constraints introduced with the chlorine substituents of chloranilic acid, $C_6Cl_2O_4H_2$, prevent parallel stacking of the ligands, and the mononuclear complex $(Bu_4N)[MoO_2(C_6Cl_2O_4)(C_6Cl_2O_4H)]$ (II) is isolated from the reaction of chloranilic acid with $(Bu_4N)_2[Mo_2O_7]$. Crystal data for I: orthorhombic space group *Pbca*, a = 15.527 (3) Å, b = 17.192 (3) Å, c = 21.094 (4) Å, Z = 4, D_{calc} = 1.54 g cm^{-3}; structure solution and refinement based on 1022 reflections ($F_o \geq 6\sigma(F_o)$; Mo Kα radiation λ = 0.710 73 Å in all cases), R = 0.060. Crystal data for II: triclinic $P\bar{1}$, a = 10.383 (2) Å, b = 13.197 (3) Å, c = 14.191 (3) Å, α = 88.11 (1)°, β = 87.57 (1)°, γ = 78.11 (2)°, Z = 2, D_{calc} = 1.37 g cm^{-3}; 4239 reflections, R = 0.055. Crystal data for III: monoclinic $P2_1/a$, a = 27.384 (5) Å, b = 10.290 (2) Å, c = 29.338 (6) Å, β = 110.98 (1)°, Z = 4, D_{calc} = 1.62 g cm^{-3}; 6125 reflections, R = 0.053. Crystal data for IV: monoclinic $P2_1/n$, a = 16.789 (3) Å, b = 9.395 (2) Å, c = 20.832 (3) Å, β = 112.72 (1)°, Z = 2, D_{calc} = 1.63 g cm^{-3}; 3030 reflections, R = 0.052.

Catechol and benzoquinone complexes of transition metals are of general interest in the investigation of ligand-centered redox processes,[1-7] in the preparation of metal semiquinone species,[8-12] and as models for metallo–biochemical processes as diverse as microbial ion transport,[13] dioxygenase activity,[14] and electron

(1) Gheller, S. F.; Newton, W. E.; de Majid, L. P.; Bradbury, J. R.; Schultz, F. A. *Inorg. Chem.* **1988**, *27*, 359. Bradbury, J. R.; Schultz, F. A. *Inorg. Chem.* **1986**, *25*, 4416.
(2) Pell, S. D.; Salmonson, R. B.; Abelliera, A.; Clarke, M. J. *Inorg. Chem.* **1984**, *23*, 385.
(3) Bowmaker, G. A.; Boyd, P. D. W.; Campbell, G. K. *Inorg. Chem.* **1982**, *21*, 2403.
(4) Harmalker, S.; Jones, S. E.; Sawyer, D. T. *Inorg. Chem.* **1983**, *22*, 2790 and references therein.
(5) Lauffer, R. B.; Heistand, R. H., II; Que, L., Jr. *J. Am. Chem. Soc.* **1981**, *103*, 3947.
(6) Buchanan, R. M.; Claflin, J.; Pierpont, C. G. *Inorg. Chem.* **1983**, *22*, 2552.
(7) Girgis, A. Y.; Sohn, Y. S.; Balch, A. L. *Inorg. Chem.* **1975**, *14*, 2327 and references therein.

0020-1669/89/1328-0723$01.50/0

transfer in bacterial photosynthesis.[15,16] More specifically, molybdenum complexes with redox-active ligands have been discussed in relation to the molybdenum hydroxylases,[17-21] enzymes characterized by the presence of an oxomolybdenum center and a pterin cofactor.[22]

The development of the coordination chemistry of molybdenum with the *o*-benzoquinone class of ligands has focused on the reactions of $[Mo(CO)_6]$ as the synthetic precursor and has revealed an extensive structural chemistry, including the binuclear oxomolybdenum(VI) species $[Mo_2O_2(dibutylcatecholate)_4]$[23] and $[Mo_2O_5(phenanthrenesemiquinone)_2]$[24] and, with tetrachloro-1,2-benzoquinone, the dimeric catecholate complex, $[Mo_2(Cl_4Cat)_6]$.[25] Furthermore, the Mo(VI)–catecholate complexes $[MoO_2(cat)_2]^{2-}$ and $[Mo_2O_5(cat)_2]^{2-}$, synthesized from reactions of catechol with conventional Mo(VI) precursors in aqueous solution, have been structurally characterized.[26-28] By exploiting the reactivity of polyoxomolybdate anions which are soluble in organic solvents,[29] we have recently extended this series to include both tetranuclear oxomolybdenum(VI) complexes of the class $[Mo_4O_{10}(OR)_2(Rcat)_2]^{2-}$[30] and ligand-bridged binuclear species $[Mo_2O_4X_4(O_4C_6X_2)_2]^{2-}$ (X = Cl and Br).[31]

As part of our investigations of the chemistry of polyoxomolybdate anions with polyhydroxybenzene and polyhydroxyquinone ligands in organic solvents, we have studied the reactions of dihydroxybenzoquinone (**1**) and its chloro derivative, chloranilic acid (**2**), tetrahydroxybenzoquinone (**3**), and 1,2,4-trihydroxybenzene (**4**) with $(n\text{-}Bu_4N)_2[Mo_2O_7]$. This paper describes the structures of the complexes $(n\text{-}Bu_4N)_2[Mo_4O_{10}(C_6H_2O_4)_2]$ (I), $(n\text{-}Bu_4N)_3[Mo_6O_{15}(C_6O_6)_2]$ (III), and $(n\text{-}Bu_4N)_2[Mo_4O_{10}(C_{12}H_4O_5)_2]$ (IV), a structurally analogous series characterized by parallel stacking of semiquinone ligands bridged by two or three $[Mo_2O_5]^{2+}$ moieties. The structure of the mononuclear chloranilate derivative $(n\text{-}Bu_4N)[MoO_2(C_6Cl_2O_4)(C_6Cl_2O_4H)]$ (II) is also described. The spectroscopic characteristics of the complexes are presented, as well as the details of their electrochemical behavior and the consequences of redox processes on the electronic and EPR spectra of I, III, and IV.

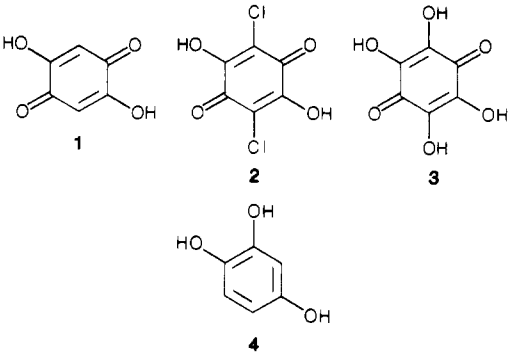

Experimental Section

Materials and Methods. All preparations were carried out in freshly distilled dry solvents, and unless otherwise noted, no precautions to eliminate atmospheric oxygen were taken. Reagent grade solvents were used throughout. $(n\text{-}Bu_4N)_2[Mo_2O_7]$ and $(n\text{-}Bu_4N)_4[Mo_8O_{26}]$ were prepared by literature methods.[32] All other reagents were obtained from standard commercial sources and used without further purification.

The following instruments were used in this work: IR, Perkin-Elmer 283B infrared spectrophotometer; UV/visible, Varian DMS 90 UV/visible spectrophotometer; electrochemistry, BAS100 electroanalytical system; EPR, Varian E4; X-ray crystallography, Nicolet R3m/V diffractometer and MicroVax II mounted solution package.

Elemental analyses were performed by Desert Analytics, Tucson, AZ.

Preparation of Compounds. **$[(C_4H_9)_4N]_2[Mo_4O_{10}(C_6H_2O_4)_2]$ (I).** 2,5-Dihydroxy-1,4-benzoquinone (0.56 g, 4 mmol) was added to a solution of $[(C_4H_9)_4N]_2[Mo_2O_7]$ (1.5 g, 2 mmol) in 30 mL of acetonitrile. After the mixture was stirred overnight, the red solution was concentrated to ca. 5 mL and layered with 10 mL of 2-propanol. After this was allowed to stand for 3 weeks at 4 °C, dark red crystals were obtained in 30% yield. Anal. Calcd for $C_{44}H_{76}N_2Mo_4O_{18}$: C, 40.5; H, 5.82; N, 2.15. Found: C, 40.7; H, 6.06; N, 2.08. IR (KBr; cm^{-1}): 2960 (m), 2880 (w), 1480 (vs), 1340 (w), 1270 (s), 1220 (vs), 950 (vs), 920 (s), 880 (m), 800 (w), 680 (m), 580 (m). UV/visible [CH_2Cl_2; λ_{max}, nm (ϵ, cm^{-1} M^{-1})]: 764 (1.8×10^3), 575 (4.4×10^3), 411 (6.8×10^3), 366 (1.6×10^4), 305 (1.5×10^4), 239 (2.7×10^4).

$[(C_4H_9)_4N][MoO_2(C_6Cl_2O_4)(C_6Cl_2O_4H)]$ (II). To a suspension of chloranilic acid (2.12 g; 10.1 mmol) in 15 mL of CH_3CN was added $(Bu_4N)_2[Mo_2O_7]$ (2.00 g, 2.54 mmol), dissolved in 15 mL of CH_3CN. The resulting intensity purple solution was stirred for 8 h at room temperature. The solution was filtered to remove an insoluble green powder, and the filterate was rotary evaporated to dryness. The residue was dissolved in 8 mL of CH_2Cl_2:DMF (3:1), and the solution was layered with 20 mL of anhydrous ether. When this was allowed to stand for 4 weeks at room temperature, the purple crystals that formed were collected by filtration, washed with ether, and dried over P_2O_5 overnight; yield 60%. Anal. Calcd for $C_{28}H_{37}Cl_4NO_{10}Mo$: C, 42.8; H, 4.72; N, 1.78. Found: C, 42.6; H, 4.59; N, 1.63. Infrared (KBr pellet, cm^{-1}): 3540 (br), 2920 (m), 2855 (w), 1650 (m) and 1630 (m) [ν(C=O)], 1570 (vs), 1550 (vs), 1345 (vs), 1290 (s), 1000 (m), 927 (s) [ν_s(Mo=O)], 900 (s)] [ν_a(Mo=O)], 830 (m), 605 (ms), 310 (m). UV/visible [CH_2Cl_2; λ_{max}, nm (ϵ, M^{-1} cm^{-1})]: 530 (1.7×10^3), 325 (2.4×10^4).

$[(C_4H_9)_4N]_3[Mo_6O_{15}(C_6O_6)_2]$ (III). Tetrahydroxy-1,4-benzoquinone (0.68 g, 4.0 mmol) was added to a solution of α-$[(C_4H_9)_4N]_4[Mo_8O_{26}]$ (2.2 g, 1.0 mmol) in 40 mL of acetonitrile. After overnight stirring, followed by concentration of the violet solution to 5 mL, 2-propanol (15 mL) was added. When this mixture was allowed to stand for 3 weeks at 4 °C, violet/black crystals of III were obtained in 25% yield. Anal. Calcd for $C_{60}H_{108}N_3Mo_6O_{27}$: C, 38.4; H, 5.75; N, 2.24. Found: C, 38.5; H, 5.96; N, 2.25. IR (KBr; cm^{-1}): 2970 (m), 2880 (w), 1425 (vs), 1375 (s), 1300 (m), 1265 (w), 1085 (s), 950 (vs), 920 (s), 800 (w), 685 (m), 600 (m). UV/visible [CH_2Cl_2; λ_{max}, nm (ϵ, cm^{-1} M^{-1})]: 719 (5.8×10^3),

(8) Mathur, P.; Dismukes, G. C. *J. Am. Chem. Soc.* **1983**, *105*, 7093.
(9) Broadley, K.; Connelly, N. G.; Geiger, W. E. *J. Chem. Soc., Dalton Trans.* **1983**, 121.
(10) Tuchagues, J.-P.; Hendrickson, D. N. *Inorg. Chem.* **1983**, *22*, 2545 and references therein.
(11) deLearie, L. A.; Pierpont, C. G. *J. Am. Chem. Soc.* **1987**, *109*, 7031 and references therein.
(12) Lynch, M. W.; Hendrickson, D. N.; Fitzgerald, B. D.; Pierpont, C. G. *J. Am. Chem. Soc.* **1984**, *106*, 2041. Buchanan, R. M.; Pierpont, C. G. *J. Am. Chem. Soc.* **1980**, *106*, 4951. Buchanan, R. M.; Kessel, S. L.; Downs, H. H.; Pierpont, C. G.; Hendrickson, D. N. *J. Am. Chem. Soc.* **1978**, *100*, 7894. Buchanan, R. M.; Downs, H. H.; Shorthill, W. B.; Pierpont, C. G.; Kessel, S. L.; Hendrickson, D. N. *J. Am. Chem. Soc.* **1978**, *100*, 4318.
(13) Raymond, K. N.; Carrano, C. J. *Acc. Chem. Res.* **1979**, *12*, 183.
(14) Que, L., Jr.; Lauffer, R. B.; Lynch, J. B.; Murch, B. P.; Pyrz, J. W. *J. Am. Chem. Soc.* **1987**, *109*, 5381. Que, L., Jr.; Kolanczyk, R. C.; White, L. S. *J. Am. Chem. Soc.* **1987**, *109*, 5373. Que, L., Jr. *Struct. Bonding (Berlin)* **1980**, *40*, 39. Que, L., Jr. *Adv. Inorg. Biochem.* **1983**, *5*, 167.
(15) Kambara, T.; Govindjee. *Proc. Natl. Acad. Sci. U.S.A.* **1985**, *88*, 6119. Govindjee; Kambara, T.; Coleman, W. *Photochem. Photobiol.* **1985**, *42*, 187. Dismukes, G. C. *Photochem. Photobiol.* **1986**, *43*, 99. Sauer, K. *Acc. Chem. Res.* **1980**, *13*, 249.
(16) Larsen, S. K.; Pierpont, C. G.; de Munno, G.; Dolcetti, G. *Inorg. Chem.* **1986**, *25*, 4828 and references therein.
(17) Garner, C. D.; Bristow, S. In *Molybdenum Enzymes*; Spiro, T. G., Ed.; Wiley: New York, 1985.
(18) Caradonna, J. P.; Reddy, P. R.; Holm, R. H. *J. Am. Chem. Soc.* **1988**, *110*, 2139.
(19) Holm, R. H. *Chem. Rev.* **1987**, *87*, 1401.
(20) Spence, J. T. *Coord. Chem. Rev.* **1983**, *48*, 59.
(21) Bray, R. C. In *The Enzymes*; Boyer, P. D., Ed.; Academic Press: New York, 1975; Vol. 12.
(22) Johnson, J. L.; Hamline, B. E.; Najagopalan, K. V.; Arison, B. H. *J. Biol. Chem.* **1984**, *259*, 5414.
(23) Pierpont, C. G.; Buchanan, R. M. *J. Am. Chem. Soc.* **1975**, *97*, 6450.
(24) Buchanan, R. M.; Pierpont, C. G. *Inorg. Chem.* **1979**, *18*, 1616.
(25) Pierpont, C. G.; Downs, H. M. *J. Am. Chem. Soc.* **1975**, *97*, 2123. Cass, M. E.; Pierpont, C. G. *Inorg. Chem.* **1986**, *25*, 122.
(26) Griffith, W. P.; Pumphrey, C. A.; Rainey, T.-A. *J. Chem. Soc., Dalton Trans.* **1986**, 1125.
(27) Atovmyan, L. O.; Sokolova, V. A.; Tkachev, V. V. *Dokl. Phys. Chem. (Engl. Transl.)* **1975**, *195*, 968. Tkachev, V. V.; Atovmyan, L. O. *Sov. J. Coord. Chem. (Engl. Trans.)* **1975**, *1*, 715.
(28) Tkachev, V. V.; Atovmyan, L. O. *Sov. J. Coord. Chem. (Engl. Trans.)* **1975**, *2*, 89.
(29) Day, V. W.; Klemperer, W. G. *Science* **1985**, *228*, 533.
(30) Liu, S.; Shaikh, S. N.; Zubieta, J. *Inorg. Chem.* **1987**, *26*, 4303.
(31) Shaikh, S. N.; Zubieta, J. *Inorg. Chim. Acta* **1988**, *146*, 149.
(32) Filowitz, M.; Ho, R. K. C.; Klemperer, W. G.; Shum, W. *Inorg. Chem.* **1979**, *18*, 93.

Table I. Summary of Crystal Parameters and Experimental Details for the Structures of $[(C_4H_9)_4N]_2[Mo_4O_{10}(C_6H_2O_4)_2]$ (I), $[(C_4H_9)_4N][MoO_2(C_6Cl_2O_4)(C_6Cl_2O_4H)]$ (II), $[(C_4H_9)_4N]_3[Mo_6O_{15}(C_6O_6)_2]$ (III), and $[(C_4H_9)_4N]_2[Mo_4O_{10}(C_{12}H_4O_5)_2]$ (IV) at 296 K

	I	II	III	IV
a, Å	15.527 (3)	10.383 (2)	27.384 (5)	16.789 (3)
b, Å	17.192 (3)	13.197 (3)	10.240 (3)	9.395 (2)
c, Å	21.094 (4)	14.191 (3)	29.338 (6)	20.832 (3)
α, deg	90.00	88.11 (1)	90.00	90.00
β, deg	90.00	87.57 (1)	110.98 (1)	112.72 (1)
γ, deg	90.00	78.11 (1)	90.00	90.00
V, Å^3	5630.6 (18)	1900.3 (11)	7718.7 (20)	3030.7 (10)
space group	*Pbca*	$P\bar{1}$	$P2_1/a$	$P2_1/n$
Z	4	2	4	2
ρ_{calc}, g cm^{-3}	1.54	1.37	1.62	1.63
radiation	Mo Kα (λ = 0.710 73 Å)			
abs coeff, cm^{-1}	8.86	6.25	9.68	8.31
T_{max}/T_{min}	1.05	1.07	1.02	1.10
final discrepancy factors				
R	0.060	0.055	0.053	0.052
R_w	0.061	0.057	0.057	0.056

530 (1.5 × 10^4), 462 (2.1 × 10^3), 330 (1.9 × 10^4), 239 (3.9 × 10^4).

$[(C_4H_9)_4N]_2[Mo_4O_{10}(C_{12}H_4O_5)_2]$ (IV). Addition of 1,2,4-trihydroxybenzene (0.5 g, 4 mmol) to a solution of α-$[(C_4H_9)_4N]_4[Mo_8O_{26}]$ (2.2 g, 1.0 mmol) in 50 mL of methanol, followed by overnight stirring, resulted in a copious brown precipitate. The crude product was dissolved in dimethylformamide (10 mL), which was layered with 25 mL of methanol. After 3 weeks, dark brown crystals of IV were obtained in 50% yield. Anal. Calcd for $C_{56}H_{80}N_2O_{20}Mo_4$: C, 45.3; H, 5.39; N, 1.89. Found: C, 45.0; H, 5.58; N, 1.92. IR (KBr; cm^{-1}): 2915 (m), 1485 (s), 1440 (vs), 1300 (vs), 1230 (m), 1200 (w), 945 (vs), 915 (m), 835 (w), 695 (m), 585 (m). UV/visible [CH_3CN; λ_{max}, nm (ϵ, cm^{-1} M^{-1})]: 833 (4.9 × 10^3), 530 (2.9 × 10^3), 439 (1.2 × 10^3), 384 (1.5 × 10^4), 230 (1.7 × 10^4).

X-ray Crystallographic Studies. The details of the crystal data, data collection methods, and refinement procedures for complexes I–IV are given in Table I and in supplementary Table S20. Full listings of bond lengths and angles, hydrogen atom coordinates, and calculated and observed structure factors for the above complexes are provided in the supplementary materials. Full details of the crystallographic methodologies may be found in ref 33.

In no instance was an extinction correction applied to the data. Idealized hydrogen atom positions were used throughout the analysis, with C–H distances set at 0.96 Å.

The $[(C_4H_9)_4N]^+$ cation of I was found to be disordered, as shown by a number of large temperature factors and a range of bond lengths, 1.34 (6)–1.65 (5) Å. A final difference Fourier map showed no peaks of electron density greater than 1.2 e/Å^3 in the region of the cation (on a scale where H atoms displayed excursions of 0.7–1.2 e/Å^3). The model was deemed adequate since the anion only was of interest and was well-behaved.

Results and Discussion

Synthesis and Spectroscopic Properties of the Complexes. Polyoxoanions that are soluble in organic solvents have been demonstrated to react with a variety of oxygen-containing ligands to yield complexes that are inaccessible by employing the conventional water-soluble polyoxoanion precursors.[29] By exploiting the reactivity of $[(C_4H_9)_4N]_2[Mo_2O_7]$ and $[(C_4H_9)_4N]_4[Mo_8O_{26}]$ in organic solvents, we have recently developed the class of oxomolybdate–catecholate complexes to include both tetranuclear oxomolybdenum(VI) complexes of the type $[Mo_4O_6(OR)_2(Rcat)_2]^{2-}$ [30] and the ligand-bridged binuclear species $[Mo_2O_4X_4(C_6X_2O_4)_2]^{2-}$ (X = Cl and Br).[31] We sought to extend this chemistry to the related series of hydroxybenzoquinone and polyhydroxybenzene derivatives dihydroxybenzoquinone (**1**), chloranilic acid (**2**), tetrahydroxybenzoquinone (**3**), and 1,2,4-trihydroxybenzene (**4**).

Reaction of $[(C_4H_9)_4N]_2[Mo_2O_7]$ with dihydroxybenzoquinone in methanol yields a bright red solution from which red blocks of $[(C_4H_9)_4N]_2[Mo_4O_{10}(C_6H_2O_4)_2]$ (*I*) crystallize over a 3-week period. A copious second crop of crystals was identified as α-$[(C_4H_9)_4N]_4[Mo_8O_{26}]$, suggesting a condensation-type reaction producing H_2O as a byproduct and resulting in reaggregation of the oxomolybdate cluster. The infrared spectrum of I is characterized by a number of features in the 580–950-cm^{-1} region, of which the strong absorbances at 950 and 920 cm^{-1} are assigned to ν_s(Mo–O$_t$) and ν_a(Mo–O$_t$), respectively. As shown in Table II, the pattern of bands is common to the infrared spectra of the structurally analogous complexes I, II, and IV (vide infra) and appears to be characteristic of the $[Mo_2O_5]^{2+}$ core bonded to oxygen donor ligands.

Table II. Comparison of Infrared Spectra[a] in the 580–950-cm^{-1} Region for the Complexes $[(C_4H_9)_4N]_2[Mo_4O_{10}(C_6H_2O_4)_2]$ (I), $[(C_4H_9)_4N]_3[Mo_6O_{15}(C_6O_6)_2]$ (III), and $[(C_4H_9)_4N]_2[Mo_4O_{10}(C_{12}H_4O_5)_2]$ (IV)

complex	ν, cm^{-1}						
I	950	920	880	830	800	684	590
III	950	920			800	688	597
IV	945	915		830	790	683	585

[a] KBr pellet.

The electronic spectrum of I is characterized by the presence of a number of charge-transfer bands with extinction coefficients in the range 10^3–10^4. The transitions at 411 nm in I and in the 410–460-nm range for the series I, III, IV may be characteristic of oxo group to metal charge transfer for the $[Mo_2O_5]^{2+}$ chromophore. The bands in the 230–330-cm^{-1} range are most likely associated with ligand n → π^* and π → π^* transitions, while the remaining features in the 500–800-nm range are attributed to transitions to the ligand-based HOMO or LUMO of the polynuclear species (vide infra).

Simple electron counting for I requires that the ligands coordinate formally as trinegative radical anions. Since the Mo(VI) oxidation state of the precursors is preserved in the products, the metal centers do not appear to participate in redox transformations of the ligand groups. Disproportionation of **1** to semiquinone forms must be invoked to account for the radical formulation of the ligands in I.

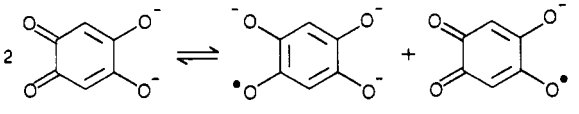

Although the ultimate fate of the unreacted semiquinone has not been established, such equilibria occur readily in quinoid chemistry and have been extensively documented.[34,35] Furthermore, the observed diamagnetism of I requires that the semiquinone ligands be magnetically coupled. The close approach of the ligand planes and parallel stacking has been confirmed crystallographically to account for the direct interaction between the radical anions.

In contrast to the chemistry of dimolybdate with **1**, reactions of $[(C_4H_9)_4N]_2[Mo_2O_7]$ and α-$[(C_4H_9)_4N]_4[Mo_8O_{26}]$ with the

(33) Bruce, A.; Corbin, J. L.; Dahlstrom, P. L.; Hyde, J. R.; Minelli, M.; Steifel, E. I.; Spence, J. T.; Zubieta, J. *Inorg. Chem.* **1982**, *21*, 917.

(34) Bernstein, J.; Cohen, M. D.; Leisenowitz, L. In *The Chemistry of the Quinoid Compounds*; Patai, I. S., Ed.; Wiley: New York, 1974; Vol. I.

(35) Baizer, M.; Lund, H. *Organic Electrochemistry*; Marcel Dekker, Inc.: New York, 1983; p 495 ff.

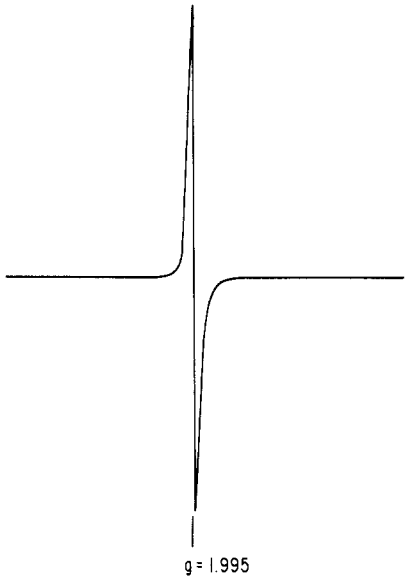

Figure 1. ESR spectrum of $(Bu_4N)_3[Mo_6O_{15}(C_6O_6)_2]$ (III) in acetonitrile at −160 °C.

chloride-substituted derivative **2**, under a variety of conditions, yielded only the intensely purple diamagnetic complex, $[(C_4H_9)_4N][MoO_2(C_6Cl_2O_4)(C_6Cl_2O_4H)]$ (II). Since II is a mononegative anion, the chloranilate ligands must be inequivalent; one ligand is present as a doubly deprotonated species while the second is singly protonated and hence mononegative. A broad peak at 3540 cm^{-1} in the infrared spectrum of II confirms the presence of an exchangeable proton on one ligand site. Furthermore, the appearance of two bands at 1650 and 1630 cm^{-1}, assigned to ν(C=O) for chemically distinct sites, confirms the inequivalence of the ligand structures. Rapid exchange apparently precluded observation of this proton in the ^1H NMR spectrum of II. On the other hand, as discussed below, the metrical parameters associated with the two ligand groups confirm the structural inequivalence and strongly suggest protonation of the uncoordinated carbonyl moieties of one chloranilate ligand.

The intense color associated with II is attributed to charge-transfer interactions, predominantly associated with the ligand itself. Indeed, solutions of **2** that have been treated with base (NEt_3) display electronic spectra similar to those of II.

The reaction of tetrahydroxybenzoquinone with α-$[(C_4H_9)_4N]_4[Mo_8O_{26}]$ in acetonitrile afforded paramagnetic violet crystals of $[(C_4H_9)_4N]_3[Mo_6O_{15}(C_6O_6)_2]$ (III). As illustrated in Tables II and XIII, the infrared spectrum and the UV/visible spectrum of III are similar to those of I, indicating that the complexes are structurally analogous. The most unusual feature of the complex is the observed paramagnetism, with a magnetic moment approaching the spin only value of 1.73 μ_B. The EPR spectrum of III shown in Figure 1 displays a narrow, single-line spectrum with g = 1.995, characteristic of an organic radical, implying that the unpaired electron is localized on the ligand. This observation is consistent with the pronounced tendency of complexes containing quinoid-type ligands to exhibit ligand-based redox processes and with the undisturbed geometry of the $[Mo_2O_5]^{2+}$ centers of the complex as shown by the crystallographic studies. One consequence of the paramagnetic trinegative formulation of the complex anion, $[Mo_6O_{15}(C_6O_6)_2]^{3-}$, is the requirement that the two $(C_6O_6)^{n-}$ ligands contribute a total charge of −9. Since the $[Mo_2O_5]^{2+}$ units are not involved in redox transformations, disproportionation of **3** to semiquinone forms must be invoked to account for the charge formalism.

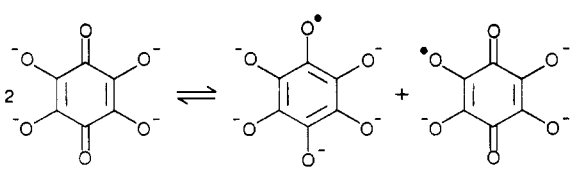

Table III. Atomic Coordinates (×10⁴) and Equivalent Isotropic Displacement Parameters (Å² × 10³) for $[(C_4H_9)_4N]_2[Mo_4O_{10}(C_6H_2O_4)_2]$

	x	y	z	U(eq)[a]
Mo	665 (1)	684 (1)	8217 (1)	83 (1)
O(1)	884 (5)	1573 (4)	8576 (5)	86 (4)
O(2)	767 (6)	1252 (4)	7126 (5)	91 (4)
O(3)	1667 (6)	356 (5)	8160 (6)	124 (5)
O(4)	0	199 (5)	7500	90 (5)
O(5)	276 (7)	450 (5)	9101 (5)	116 (4)
C(1)	923 (7)	2045 (7)	8109 (7)	71 (5)
C(2)	890 (7)	1848 (7)	7279 (7)	76 (5)
C(3)	968 (8)	2327 (7)	6695 (7)	70 (5)
N(1)	2500	0	5609 (8)	81 (6)
C(11)	2290 (21)	438 (16)	4921 (20)	103 (9)
C(12)	1709 (22)	978 (16)	5084 (18)	120 (10)
C(13)	1191 (34)	1325 (24)	4521 (29)	174 (18)
C(14)	814 (41)	1871 (33)	4393 (37)	139 (22)
C(15)	3264 (20)	322 (14)	5875 (17)	89 (8)
C(16)	3049 (31)	811 (19)	6488 (25)	106 (13)
C(17)	4042 (39)	1245 (31)	6463 (40)	155 (23)
C(18)	4022 (54)	1729 (39)	7076 (50)	166 (29)

[a] Equivalent isotropic U defined as one-third of the trace of the orthogonalized U_{ij} tensor.

The unexpected product of the reaction of α-$[(C_4H_9)_4N]_4[Mo_8O_{26}]$ with 1,2,4-trihydroxybenzene (**4**) was $[(C_4H_9)_4N]_2[Mo_4O_{10}(C_{12}H_4O_5)_2]$ (IV), a complex structurally analogous to I and III and containing tetraoxydibenzofuran units. The formation of $(C_{12}H_4O_5)^{n-}$ moieties from **4** may be rationalized in terms of the ubiquitous para-phenolic coupling reaction, a radical mechanism invoked in the synthesis of bisphenol A, which may be generally represented

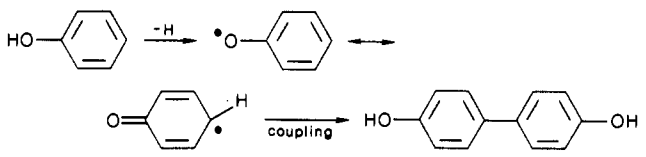

In the specific case of **4**, the only available para site dictates the mode of coupling. We speculate that the intermediate undergoes metal-assisted dehydration

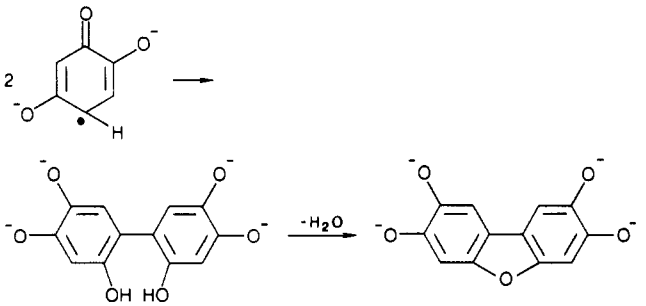

to yield the dibenzofuran unit of the product. In common with the ligand behavior in I and III, the $(C_{14}H_4O_5)^{n-}$ groups of IV adopt semiquinone oxidation states to account for the charge requirements of the complex. The observed diamagnetism implies strong magnetic coupling of the radical anion sites.

Description of the Structures. Atomic positional parameters for the structures of I–IV are tabulated in Tables III, V, VII, and IX, respectively, while Tables IV, VI, VIII, and X list selected bond lengths and angles for the structures.

As shown in Figure 2, the structure of I consists of discrete tetranuclear dinegative molecular anions, $[Mo_4O_{10}(C_6H_2O_4)_2]^{2-}$, with 2-fold axes passing through O(4) and O(4a) and through the midpoints of the phenyl rings generating the symmetry related portions of the tetrametallic cluster. The $(C_6H_2O_4)^{n-}$ ligands function as chelating tetradentate groups bridging two $[Mo_2O_5]^{2+}$ units.

The Mo coordination sites in I consist of two sets of two distorted $[MoO_6]$ octahedra sharing a common face to give a con-

Table IV. Selected Bond Lengths (Å) and Angles (deg) for $[(C_4H_9)_4N]_2[Mo_4O_{10}(C_6H_2O_4)_2]$ (I)

Mo(1)–O(1)	2.003 (9)	Mo(1)–O(2a)	2.594 (8)
Mo(1)–O(2)	2.232 (9)	Mo–Mo(a)	3.216 (1)
Mo(1)–O(3)	1.705 (9)	O(1)–C(1)	1.28 (1)
Mo(1)–O(4)	1.906 (6)	O(2)–C(1)	1.30 (1)
Mo(1)–O(5)	1.708 (9)		
O(1)–Mo–O(2)	75.2 (3)	O(3)–Mo–O(5)	104.9 (5)
O(1)–Mo–O(3)	104.1 (4)	O(3)–Mo–O(2a)	163.0 (5)
O(1)–Mo–O(4)	142.5 (4)	O(4)–Mo–O(5)	103.3 (4)
O(1)–Mo–O(5)	93.2 (4)	O(4)–Mo–O(2a)	68.7 (4)
O(1)–Mo–O(2a)	77.5 (4)	O(5)–Mo–O(2a)	91.9 (4)
O(2)–Mo–O(3)	96.0 (4)	Mo–O(4)–Mo(a)	115.1 (2)
O(1)–Mo–O(4)	77.4 (3)	Mo–O(2)–Mo(a)	83.2 (2)
O(2)–Mo–O(5)	158.1 (4)	Mo–O(1)–C(1)	122.9 (8)
O(2)–Mo–O(2a)	67.8 (4)	Mo–O(2)–C(2)	111.1 (8)
O(3)–Mo–O(4)	103.9 (4)		

Table V. Atomic Coordinates ($\times 10^4$) and Equivalent Isotropic Displacement Parameters ($Å^2 \times 10^3$) for $(Bu_4N)[MoO_2(C_6Cl_2O_4)(C_6Cl_2O_4H)]$

	x	y	z	U(eq)[a]
Mo	629 (1)	3226 (1)	2711 (1)	46 (1)
Cl(1)	2009 (2)	5261 (2)	96 (1)	67 (1)
Cl(2)	6669 (2)	8668 (2)	159 (2)	75 (1)
Cl(3)	9057 (2)	9680 (2)	2751 (2)	74 (1)
Cl(4)	6549 (2)	8972 (2)	4889 (2)	84 (1)
O(1)	11719 (6)	4033 (4)	2732 (4)	64 (2)
O(2)	9334 (5)	3812 (4)	3395 (4)	63 (2)
O(3)	9552 (5)	3715 (4)	1550 (3)	50 (2)
O(4)	11766 (5)	2413 (4)	1516 (3)	53 (2)
O(5)	11757 (5)	2271 (4)	3643 (3)	53 (2)
O(6)	9945 (5)	1765 (4)	2735 (3)	53 (2)
O(7)	9523 (6)	3739 (5)	−1767 (4)	85 (3)
O(8)	11777 (6)	2319 (5)	−1811 (4)	85 (3)
O(9)	12554 (7)	−954 (5)	5214 (5)	89 (3)
O(10)	10644 (7)	−1531 (4)	4257 (4)	81 (3)
C(1)	10504 (7)	1043 (5)	3291 (5)	45 (2)
C(2)	10223 (8)	56 (6)	3408 (5)	56 (3)
C(3)	10865 (8)	−666 (6)	4085 (6)	62 (3)
C(4)	11976 (8)	−341 (6)	4659 (5)	59 (3)
C(5)	12218 (7)	679 (6)	4485 (5)	52 (3)
C(6)	11545 (6)	1337 (5)	3841 (4)	44 (2)
C(7)	11313 (7)	2652 (5)	686 (5)	47 (2)
C(8)	11866 (7)	2255 (6)	−147 (5)	51 (3)
C(9)	11295 (8)	2605 (6)	−1011 (5)	57 (3)
C(10)	10015 (8)	3442 (6)	−999 (5)	58 (3)
C(11)	9430 (7)	3808 (5)	−108 (5)	50 (3)
C(12)	10011 (7)	3440 (5)	701 (5)	45 (2)
N(1)	5820 (6)	2596 (4)	2231 (4)	52 (2)
C(13)	5080 (8)	3638 (6)	1860 (6)	60 (3)
C(14)	5762 (8)	4528 (6)	1953 (6)	64 (3)
C(15)	4982 (10)	5518 (7)	1489 (7)	82 (4)
C(16)	5606 (14)	6438 (9)	1576 (9)	125 (6)
C(17)	4843 (8)	1872 (6)	2236 (6)	59 (3)
C(18)	5386 (8)	734 (6)	2524 (6)	65 (3)
C(19)	4380 (9)	98 (7)	2336 (6)	72 (3)
C(20)	4725 (10)	−977 (7)	2716 (7)	87 (4)
C(21)	6333 (10)	2683 (6)	3200 (6)	80 (4)
C(22)	5313 (14)	3090 (9)	3952 (7)	38 (4)
C(23)	6243 (16)	3431 (12)	4796 (11)	56 (6)
C(24)	5367 (24)	3414 (15)	5236 (23)	172 (28)
C(25)	7041 (7)	2195 (6)	1624 (6)	65 (3)
C(26)	6826 (10)	1945 (8)	615 (7)	84 (4)
C(27)	8089 (13)	1392 (11)	160 (10)	126 (6)
C(28)	8139 (18)	1203 (14)	−741 (13)	214 (13)
C(41)	−459 (9)	6879 (6)	3610 (5)	61 (3)
C(42)	650 (14)	6177 (9)	3993 (8)	46 (5)
O(11)	−1682 (15)	6599 (10)	3911 (9)	92 (6)

[a] Equivalent isotropic U defined as one-third of the trace of the orthogonalized U_{ij} tensor.

facial bioctahedral geometry.[36] The Mo–O distances adopt a modified 2 + 2 + 2 pattern, that is, two short, two intermediate and two long distances with ranges of 1.68–1.71, 1.90–2.04, and 2.23–2.59 Å, respectively. The metrical parameters associated with the $[Mo_2O_5]^{2+}$ core are similar to those observed for $[Mo_2O_5(C_2O_4)_2(H_2O)_2]^{2-}$[37] and the closely related catecholate

(36) Cotton, F. A.; Ucko, D. A. *Inorg. Chim. Acta* **1972**, *6*, 161.

Table VI. Selected Bond Lengths (Å) and Angles (deg) for $[(C_4H_9)_4N][MoO_2(C_6Cl_2O_4)(C_6Cl_2O_4H)]$ (II)

Mo–O(1)	1.709 (5)	Mo–O(4)	2.202 (5)
Mo–O(2)	1.691 (5)	Mo–O(5)	2.030 (5)
Mo–O(3)	2.043 (5)	Mo–O(6)	2.187 (5)
C(1)–O(6)	1.276 (8)	C(7)–O(4)	1.292 (8)
C(6)–O(5)	1.317 (8)	C(12)–O(3)	1.311 (8)
C(1)–C(6)	1.480 (8)	C(7)–C(12)	1.526 (9)
C(1)–C(2)	1.396 (10)	C(7)–C(8)	1.364 (9)
C(2)–C(3)	1.417 (11)	C(8)–C(9)	1.407 (10)
C(3)–C(4)	1.577 (12)	C(9)–C(10)	1.543 (11)
C(4)–C(5)	1.431 (11)	C(10)–C(11)	1.435 (10)
C(5)–C(6)	1.352 (9)	C(11)–C(12)	1.348 (9)
C(4)–O(9)	1.196 (9)	C(9)–O(8)	1.240 (9)
O(1)–Mo–O(2)	104.1 (3)	Mo–O(3)–Cl(12)	121.1 (4)
O(1)–Mo–O(6)	158.0 (2)	Mo–O(4)–C(7)	116.8 (4)
O(2)–Mo–O(4)	160.5 (2)	Mo–O(5)–C(6)	120.7 (4)
O(3)–Mo–O(5)	160.3 (2)	Mo–O(6)–C(1)	117.4 (4)
O(3)–Mo–O(4)	74.4 (2)		
O(5)–Mo–O(6)	73.8 (2)		

Table VII. Atomic Coordinates ($\times 10^4$) and Equivalent Isotropic Displacement Parameters ($Å^2 \times 10^3$) for $[(C_4H_9)_4N]_3[Mo_6O_{15}(C_6O_6)_2]$

	x	y	z	U(eq)[a]
Mo(1)	182 (1)	1513 (1)	1957 (1)	65 (1)
Mo(2)	−73 (1)	−770 (1)	1165 (1)	68 (1)
Mo(3)	1877 (1)	−3081 (1)	1564 (1)	73 (1)
Mo(4)	1977 (1)	−5055 (1)	2427 (1)	73 (1)
Mo(5)	1977 (1)	−1782 (1)	3949 (1)	71 (1)
Mo(6)	764 (1)	−1263 (1)	3708 (1)	68 (1)
O(1)	30 (2)	−908 (7)	1957 (2)	56 (3)
O(2)	414 (2)	−2278 (7)	1428 (3)	62 (3)
O(3)	1275 (3)	−4038 (7)	1908 (3)	63 (3)
O(4)	1596 (3)	−4339 (7)	2849 (3)	65 (3)
O(5)	1157 (3)	−2784 (6)	3417 (2)	57 (3)
O(6)	382 (2)	−1225 (7)	2983 (2)	59 (3)
O(7)	766 (3)	996 (6)	2583 (2)	61 (3)
O(8)	752 (2)	416 (7)	1721 (2)	60 (3)
O(9)	1472 (2)	−1480 (7)	1606 (3)	62 (3)
O(10)	2122 (3)	−2633 (7)	2376 (3)	66 (3)
O(11)	2133 (2)	−1981 (7)	3331 (3)	64 (3)
O(12)	1465 (3)	−318 (6)	3426 (3)	61 (3)
O(13)	−260 (3)	1712 (7)	2230 (3)	79 (4)
O(14)	367 (3)	3026 (7)	1869 (3)	84 (4)
O(15)	−660 (3)	−1522 (9)	946 (3)	88 (4)
O(16)	109 (3)	−561 (9)	679 (3)	95 (4)
O(17)	1480 (3)	−3534 (8)	995 (3)	90 (4)
O(18)	2396 (3)	−2371 (8)	1487 (3)	90 (4)
O(19)	1753 (3)	−6592 (8)	2342 (3)	94 (4)
O(20)	2572 (3)	−5149 (8)	2879 (3)	91 (4)
O(21)	2214 (3)	−3269 (8)	4172 (3)	94 (4)
O(22)	2458 (3)	−749 (8)	4275 (3)	91 (4)
O(23)	369 (3)	−2265 (8)	3876 (3)	89 (4)
O(24)	578 (3)	254 (8)	3801 (3)	89 (4)
O(25)	−234 (3)	950 (7)	1317 (3)	74 (3)
O(26)	2157 (3)	−4694 (8)	1863 (3)	85 (4)
O(27)	1439 (3)	−1461 (7)	4203 (2)	79 (3)
C(1)	372 (3)	−1791 (10)	2186 (3)	48 (4)
C(2)	592 (4)	−2544 (10)	1899 (4)	50 (4)
C(3)	1006 (4)	−3404 (10)	2130 (4)	55 (4)
C(4)	1191 (4)	−3566 (10)	2647 (4)	56 (5)
C(5)	977 (4)	−2830 (10)	2943 (4)	51 (4)
C(6)	550 (3)	−1955 (10)	2699 (4)	54 (4)
C(7)	1128 (4)	186 (10)	2556 (4)	55 (5)
C(8)	1129 (3)	−128 (10)	2083 (4)	54 (4)
C(9)	1484 (4)	−1063 (11)	2042 (4)	60 (5)
C(10)	1845 (4)	−1708 (11)	2458 (4)	59 (5)
C(11)	1839 (4)	−1379 (10)	2927 (4)	59 (5)
C(12)	1478 (4)	−462 (10)	2984 (4)	56 (5)

[a] Equivalent isotropic U defined as one-third of the trace of the orthogonalized U_{ij} tensor.

Table VIII. Selected Bond Lengths (Å) and Angles (deg) for $[(C_4H_9)_4N]_3[Mo_6O_{15}(C_6O_6)_2]$ (III)

Mo(1)···Mo(2)	3.201 (2)			Mo(3)···Mo(4)	3.178 (1)			Mo(5)···Mo(6)	3.184 (1)		
Mo(1)–O(1)	2.526 (7)	Mo(2)–O(8)	2.572 (7)	Mo(3)–O(3)	2.428 (7)	Mo(4)–O(10)	2.536 (7)	Mo(5)–O(5)	2.454 (7)	Mo(6)–O(12)	2.541 (7)
Mo(1)–O(7)	2.027 (6)	Mo(2)–O(2)	2.011 (7)	Mo(3)–O(9)	2.013 (7)	Mo(4)–O(4)	2.063 (7)	Mo(5)–O(11)	2.017 (7)	Mo(6)–O(6)	2.008 (7)
Mo(1)–O(8)	2.229 (7)	Mo(2)–O(1)	2.242 (6)	Mo(5)–O(10)	2.277 (7)	Mo(4)–O(3)	2.238 (7)	Mo(5)–O(12)	2.246 (6)	Mo(6)–O(5)	2.234 (7)
Mo(1)–O(13)	1.684 (7)	Mo(2)–O(15)	1.691 (8)	Mo(5)–O(17)	1.701 (8)	Mo(4)–O(19)	1.682 (8)	Mo(5)–O(21)	1.699 (7)	Mo(6)–O(25)	1.690 (7)
Mo(1)–O(14)	1.686 (7)	Mo(2)–O(16)	1.683 (7)	Mo(3)–O(18)	1.685 (7)	Mo(4)–O(20)	1.696 (8)	Mo(5)–O(22)	1.697 (7)	Mo(6)–O(24)	1.694 (8)
Mo(1)–O(25)	1.905 (7)	Mo(2)–O(25)	1.915 (7)	Mo(3)–O(26)	1.905 (7)	Mo(4)–O(26)	1.923 (7)	Mo(5)–O(27)	1.904 (8)	Mo(6)–O(27)	1.908 (2)
O(1)–C(1)	1.306 (10)	O(2)–C(2)	1.319 (11)	O(3)–C(3)	1.306 (10)	O(4)–C(4)	1.320 (11)	O(5)–C(5)	1.302 (10)	O(6)–C(6)	1.320 (11)
O(7)–C(7)	1.318 (11)	O(8)–C(8)	1.313 (10)	O(9)–C(9)	1.338 (12)	O(10)–C(10)	1.293 (12)	O(11)–C(11)	1.323 (11)	O(12)–C(12)	1.319 (12)
O(1)–Mo(1)–O(14)		165.8 (3)		O(3)–Mo(3)–O(18)		164.4 (3)		O(5)–Mo(5)–O(22)		166.0 (3)	
O(7)–Mo(1)–O(25)		144.3 (3)		O(9)–Mo(3)–O(26)		145.6 (3)		O(11)–Mo(5)–O(27)		144.4 (3)	
O(8)–Mo(1)–O(13)		155.7 (3)		O(10)–Mo(3)–O(17)		158.2 (3)		O(12)–Mo(5)–O(21)		157.8 (3)	
O(7)–Mo(1)–O(8)		74.6 (3)		O(9)–Mo(3)–O(10)		74.6 (3)		O(11)–Mo(5)–O(12)		74.6 (3)	
O(1)–Mo(1)–O(25)		70.1 (3)		O(3)–Mo(3)–O(26)		71.2 (3)		O(5)–Mo(5)–O(27)		70.2 (3)	
Mo(1)–O(1)–Mo(2)		84.1 (2)		Mo(3)–O(3)–Mo(4)		85.8 (2)		Mo(5)–O(5)–Mo(6)		85.4 (2)	
Mo(1)–O(8)–Mo(2)		83.3 (2)		Mo(3)–O(10)–Mo(4)		82.5 (2)		Mo(5)–O(12)–Mo(6)		83.1 (2)	
Mo(1)–O(25)–Mo(2)		113.9 (3)		Mo(3)–O(26)–Mo(4)		112.3 (3)		Mo(5)–O(27)–Mo(6)		113.2 (3)	
O(8)–Mo(2)–O(15)		163.4 (3)		O(10)–Mo(4)–O(19)		166.3 (3)		O(12)–Mo(6)–O(23)		164.9 (3)	
O(2)–Mo(2)–O(25)		143.1 (3)		O(4)–Mo(4)–O(26)		143.5 (3)		O(6)–Mo(6)–O(21)		143.4 (3)	
O(1)–Mo(2)–O(16)		157.0 (2)		O(3)–Mo(4)–O(20)		158.2 (3)		O(5)–Mo(6)–O(24)		156.9 (3)	
O(1)–Mo(2)–O(2)		74.5 (3)		O(3)–Mo(4)–O(4)		75.0 (3)		O(5)–Mo(6)–O(6)		75.4 (3)	
O(8)–Mo(2)–O(15)		68.7 (3)		O(10)–Mo(4)–O(26)		70.5 (3)		O(12)–Mo(6)–O(27)		69.5 (3)	

Table IX. Atomic Coordinates ($\times 10^4$) and Equivalent Isotropic Displacement Parameters ($Å^2 \times 10^3$) for $[(C_4H_9)_4N]_2[Mo_4O_{10}(C_{12}H_4O_5)_2]$

	x	y	z	U(eq)[a]
Mo(1)	3126 (1)	−1980 (1)	4881 (1)	42 (1)
Mo(2)	1582 (1)	328 (1)	4328 (1)	41 (1)
O(1)	2755 (3)	−129 (5)	4523 (3)	43 (2)
O(2)	3433 (4)	−2718 (6)	4270 (3)	61 (3)
O(3)	4058 (3)	−1643 (6)	5569 (3)	61 (3)
O(4)	1673 (4)	1609 (6)	4925 (3)	52 (2)
O(5)	1269 (4)	1174 (6)	3554 (3)	62 (3)
O(6)	2760 (3)	−3840 (5)	5165 (3)	44 (2)
O(7)	2190 (3)	−1402 (5)	5366 (3)	41 (2)
O(8)	463 (3)	−449 (5)	4298 (3)	42 (2)
O(9)	1566 (3)	−1952 (5)	4016 (3)	41 (2)
O(10)	−70 (3)	−6190 (5)	3988 (3)	39 (2)
C(1)	2157 (4)	−3892 (8)	5433 (3)	35 (3)
C(2)	1817 (4)	−2506 (8)	5518 (4)	37 (3)
C(3)	1125 (5)	−2397 (8)	5743 (4)	38 (3)
C(4)	790 (4)	−3685 (8)	5843 (3)	34 (3)
C(5)	1109 (4)	−5039 (8)	5756 (3)	34 (3)
C(6)	1823 (4)	−5139 (8)	5560 (4)	34 (3)
C(7)	266 (5)	−1832 (8)	4179 (4)	38 (3)
C(8)	905 (5)	−2684 (8)	4038 (4)	38 (3)
C(9)	809 (5)	−4163 (8)	3938 (4)	37 (3)
C(10)	103 (5)	−4734 (8)	4012 (3)	35 (3)
C(11)	−533 (4)	−3947 (8)	4153 (4)	34 (3)
C(12)	−456 (5)	−2441 (8)	4223 (4)	36 (3)

[a] Equivalent isotropic U defined as one third of the trace of the orgonalized U_{ij} tensor.

Table X. Selected Bond Lengths (Å) and Angles (deg) for $[(C_4H_9)_4N]_2[Mo_4O_{10}(C_{12}H_4O_5)_2]$ (IV)

Mo(1)···Mo(2)	3.232 (1)		
Mo(1)–O(1)	1.900 (5)	Mo(2)–O(1)	1.899 (5)
Mo(1)–O(2)	1.694 (6)	Mo(2)–O(4)	1.674 (5)
Mo(1)–O(3)	1.694 (6)	Mo(2)–O(5)	1.689 (6)
Mo(1)–O(6)	2.015 (5)	Mo(2)–O(8)	1.993 (5)
Mo(1)–O(7)	2.239 (4)	Mo(2)–O(9)	2.235 (5)
Mo(1)–O(9)	2.542 (5)	Mo(2)–O(7)	2.580 (5)
O(6)–C(1)	1.332 (8)	O(8)–C(7)	1.340 (9)
O(7)–C(2)	1.313 (9)	O(9)–C(8)	1.320 (8)
O(3)–Mo(1)–O(9)	163.7 (2)	O(5)–Mo(1)–O(7)	166.7 (2)
O(1)–Mo(1)–O(6)	144.8 (2)	O(1)–Mo(2)–O(8)	144.1 (2)
O(2)–Mo(1)–O(7)	155.3 (2)	O(4)–Mo(2)–O(9)	151.8 (2)
O(6)–Mo(1)–O(7)	74.4 (2)	O(8)–Mo(2)–O(9)	74.6 (2)
O(1)–Mo(1)–O(9)	67.7 (2)	O(1)–Mo(2)–O(7)	68.7 (2)
Mo(1)–O(1)–Mo(2)	116.5 (2)	Mo(1)–O(9)–Mo(2)	84.9 (2)
Mo(1)–O(7)–Mo(2)	83.9 (2)		

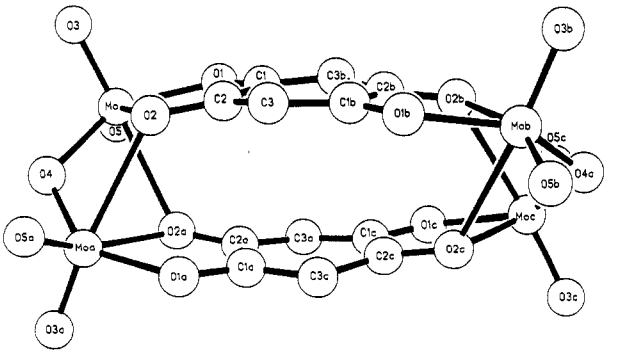

Figure 2. ORTEP view of the structure of the molecular anion of $(Bu_4N)_2[Mo_4O_{10}(C_6H_2O_4)_2]$ (I), showing the atom-labeling scheme.

and semiquinone complexes $[Mo_2O_5(3,5\text{-DBcat})_2]^{2-}$[23] and $[Mo_2O_5(C_{14}H_8O_2)_2]$.[24] The terminal oxo ligands adopt the usual cis geometry with short Mo–O distances, while the bridging oxo group displays an intermediate Mo–O(4) distance of 1.906 (6)

(37) Cotton, F. A.; Morehouse, S. M.; Wood, J. S. *Inorg. Chem.* **1964**, *3*, 1603.

Table XI. Comparison of Structural Parameters for the $[Mo_2O_9]$ Cores of the Complexes of This Study and of Related Pentaoxodimolybdate–Bis(semiquinone) Type Structures

	I	III	IV	$[Mo_2O_5(C_{14}H_8O_2)_2]$	$[Mo_2O_5(3,5\text{-DBcat})_2]^{2-}$
$Mo-O_t$[a]	1.707 (10)	1.691 (9)	1.693 (7)	1.686 (8)	1.700 (14)
$Mo-O_b$	1.906 (6)	1.910 (9)	1.904 (5)	1.904 (8)	1.919 (19)
$Mo-O_x$	2.003 (9)	2.017 (9)	2.004 (7)	2.041 (9)	1.977 (12)
$Mo-O_y$	2.232 (9)	2.244 (8)	2.37 (8)	2.242 (2)	2.156 (12)
$Mo-O_z$	2.594 (8)	2.509 (9)	2.561 (8)	2.495 (7)	2.385 (12)
O_x-Mo-O_y	75.2 (3)	74.8 (8)	74.5 (3)	73.9 (3)	75.8 (6)
$Mo-O_b-Mo$	115.1 (2)	113.1 (5)	116.5 (2)	112.7 (2)	109.4 (4)
$Mo-O_y-Mo$	83.2 (3)	83.0 (6)	83.9 (2)	83.0 (1)	86.5 (3)
$Mo-O_z-Mo$	83.2 (3)	85.1 (5)	84.9 (2)	84.0 (1)	87.6 (3)
ref	b	*b*	*b*	23	37

[a] Abbreviations: O_t, terminal oxo group-, O_b, bridging oxo group; O_x, ligand oxygen donor coordinated to a single Mo center; O_y and O_z, ligand oxygen donor bridging two Mo sites. The $Mo-O_x$ and $Mo-O_y$ distances refer to oxygen donors within a single chelate unit $[Mo-O_x-C-C-O_y]$, whereas the $Mo-O_z$ distances refer specifically to the quinone oxygen donor bridging from the adjacent [Mo–O–C–C–O] chelate ring. [b] This work.

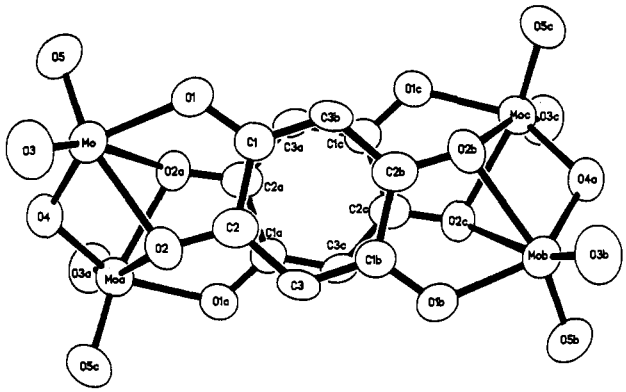

Figure 3. View of the structure of $[Mo_4O_{10}(C_6H_2O_4)_2]^{2-}$ normal to the ring plane, showing the staggered configuration of the rings.

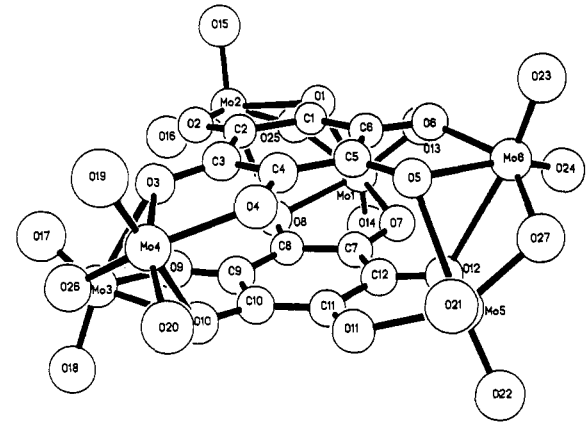

Figure 4. ORTEP view of the structure of $[Mo_6O_{15}(C_6O_6)_2]^{3-}$, viewed normal to the ring plane to illustrate the staggered orientation of the rings.

Å. The $(C_6H_2O_4)^{n-}$ ligands bond terminally through the O(1) donor types, while the O(2) donors bridge the metals unsymmetrically. As anticipated, the terminal oxo groups exert a significant trans influence, such that the Mo–O(2) and Mo–O(2a) distances of 2.232 (9) and 2.594 (8) Å are considerably longer than the Mo–O(1) distance of 2.003 (9) Å, for the oxygen donor trans to the bridging oxo group O(4). The Mo–O distances to semiquinone oxygen donors associated in the chelate ring interaction [Mo–O–C–C–O] are significantly shorter (2.003 (9) Å, 2.232 (9) Å) than that for the weakly bridging interaction with the oxygen donor of the adjacent chelate (2.594 (8) Å). The long Mo···Mo distance of 3.216 (1) Å is consistent with the absence of metal–metal interaction in a binuclear Mo(VI) species.

As illustrated by Table XI, the metrical parameters associated with the $[Mo_2O_9]$ moieties of I are similar to those observed for III and IV of this work and for the previously reported structures $[Mo_2O_5(C_{14}H_8O_2)_2]$ and $[Mo_2O_5(3,5\text{-DBcat})_2]^{2-}$.[38] Since the oxidation levels of these complexes differ by one or two electrons, this observation suggests that the HOMO's are ligand based, such that the $[Mo_2O_5]^{2+}$ metal cores are not involved in the redox chemistries of these species. These structural results appear to confirm the spectroscopic assignments and also support the electrochemical observations discussed below.

The charge requirements for I, as previously noted, dictate that the $(C_6H_2O_4)^{n-}$ ligands coordinate formally as radical anions. This formulation is consistent with the C–O bond lengths which average 1.29 (1) Å, intermediate between values of 1.22 Å found for benzoquinones and 1.38 Å for hydroquinones.[34] The analogous $[Mo_2O_5(C_{14}H_8O_2)_2]$ exhibits C–O distances of 1.313 (8) Å.

Since the complex is diamagnetic, the ligands must be magnetically coupled. The crystallographically imposed parallel orientation of the quinoid ligands in I, together with the staggered ring configuration shown in Figure 3, suggests direct interaction between radical anions. The interplanar separation of 2.67 Å is extremely short compared to 3.15 Å for TCNQ molecules in conductive crystals[39] and may be compared to an interplanar separation of ca. 3.10 Å in $[Mo_2O_5(C_{14}H_8O_2)_2]$, an analogous complex that also exhibits magnetic coupling of semiquinone radical anions.[23]

The gross structural features associated with III and IV are similar to those observed for I. The structure of III, illustrated in Figure 4, consists of three $[Mo_2O_5]^{2+}$ units, bridged by chelating hexadentate $(C_6O_6)^{n-}$ ligands. The three $[Mo_2O_9]$ coordination moieties of III exhibit metrical parameters nearly identical with those observed for I, IV, and related complexes listed in Table XI. Furthermore, III presents the staggered parallel ring orientation of the two (C_6O_6) units and a short interplanar distance of 2.705 Å. This interplanar separation is consistent with direct interaction of the ligand ring systems, providing a mechanism for magnetic coupling, a feature that is consistent with the redox behavior and magnetic properties of III, as discussed below.

Two views of the structure of the dinegative anion of IV are presented in Figure 5. In gross structural features, IV is related to I by replacement of the $(C_6H_2O_4)$ ligand moieties by tetraoxydibenzofuran groups, $(C_{12}H_4O_5)$. Although the parallel staggered ring geometry of the ligands is maintained for the $(C_{12}H_4O_5)$ units of IV, the interplanar separation has increased to 3.354 Å for the central (C_4O) furanyl unit, in contrast to interplanar distances of ca. 2.70 Å for I and III. The $(C_{12}H_4O_5)$ units are distinctly bowed, such that the donor group O···O interligand distances are ca. 2.80 Å. The observed diamagnetism of the complex indicates that strong magnetic coupling is maintained, despite the somewhat larger separation of the ligand planes.

The short interplanar separations of the semiquinone ligands of I, III, and IV suggest that steric constraints may dramatically affect the degree of aggregation achieved through parallel stacking of bridging semiquinoid units. Chloranilic acid (**2**) is structurally related to **1** and **3** by substitution of bulky chloro groups for the

(38) Pierpont, C. G.; Buchanan, R. M. *Inorg. Chem.* **1982**, *21*, 652.

(39) Garito, A. F.; Heeger, A. J. *Acc. Chem. Res.* **1974**, *7*, 232.

Table XII. Electrochemical Parameters of Complexes Containing $[Mo_2O_5]^{2+}$ Units Bridged by Quinoid Ligands

complex	$E_{1/2}$,[a] V	E_p-E_p,[b] mV	$(i_p/i_p)^c$	i_p/cv,[d] A $s^{1/2}$ M^{-1} $V^{-1/2}$	n[e]
$(Bu_4N)_2[Mo_4O_{10}(C_6H_2O_4)_2]$	−0.208 (r)	60	1.0	1.3	1.0
	−0.677 (r)	61	1.0	1.3	1.0
$(Bu_4N)_3[Mo_6O_{15}(C_6O_6)_2]$	+0.428 (o)	59	1.0	1.3	1.0
	−0.010 (r)	61	1.0	1.2	1.0
$(Bu_4N)_2[Mo_4O_{10}(C_{12}H_4O_5)_2]$	+0.170 (r)	63	1.0	1.2	1.0
	−0.140 (r)	64	1.0	1.1	1.0
	−0.352 (r)	87	3.2	2.1	*ca.* 2.0

[a] SCE ±0.01. Estimated by cyclic voltammetry from $E_{1/2} = (E_p - E_p)/2 = E_p - 29$ mV. The shape parameter $E_p - E_p$ lay within the range 60–80 mV for all the complexes. The notation in parentheses refers to the nature of the redox process: r = reduction; o = oxidation. [b] ±5. [c] Peak current ratio at 250 mV/s. i_p is proportional to $V^{1/2}$ over the range 0.01 to 1.0 V/s for 5×10^{-3} M solutions of complexes. [d] The value observed for the ferrocene/ferrocenium couple at the same electrode is 1.3 A $s^{1/2}$ M^{-1} $V^{-1/2}$. [e] Confirmed by controlled-jpotential electrolyses.

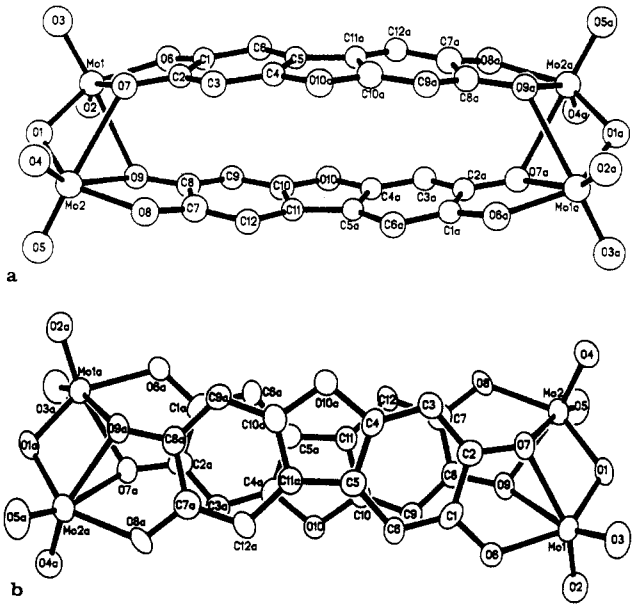

Figure 5. (a) ORTEP view of the structure of $[Mo_4O_{10}(C_{12}H_4O_5)_2]^{2-}$ (IV), showing the atom-labeling scheme. (b) View of the structure of IV normal to the ring plane.

H atoms or two OH groups of **1** and **3**, respectively. The only product isolated from the reactions of **2** with polyoxomolybdates under a variety of conditions was the mononuclear complex $[(C_4H_9)_4N][MoO_2(C_6Cl_2O_4)(C_6Cl_2O_4H)]$ (II), suggesting that the steric and repulsive effects associated with the Cl substituents prevent the usual parallel stacking of the ligands.

As shown in Figure 6, II displays the *cis*-dioxo geometry characteristic of mononuclear Mo(VI) complexes with pseudooctahedral $[MoO_6]$ coordination geometry. The trans influence of the oxo groups is evident in the nonequivalent Mo–O(ligand) distances, averaging 2.037 (6) and 2.195 (6) Å for ligation cis and trans to the oxo groups, respectively. The 2 + 2 + 2 pattern of Mo–O distances is evident in the bonding parameters for II presented in Table VI.

Since II is a mononegative anion, one chloranilate ligand must be present as the doubly deprotonated $(C_6Cl_2O_4)^{2-}$ groups while the second is singly protonated $(C_6Cl_2O_4H)^-$. This feature appears to be reflected in the structural parameters associated with the nonequivalent ligand sites. The pattern of bond lengths

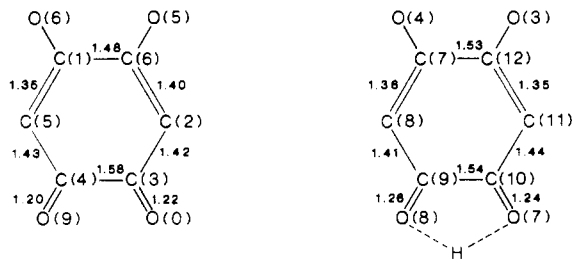

is consistent with localization of single-bond character in the

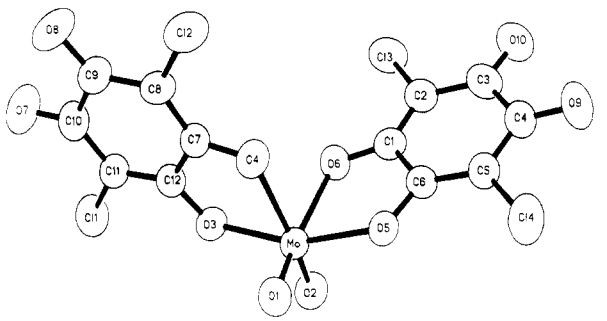

Figure 6. Perspective view of the structure of $[MoO_2(C_6Cl_2O_4)(C_6Cl_2O_4H)]^-$ showing the atom-labeling scheme.

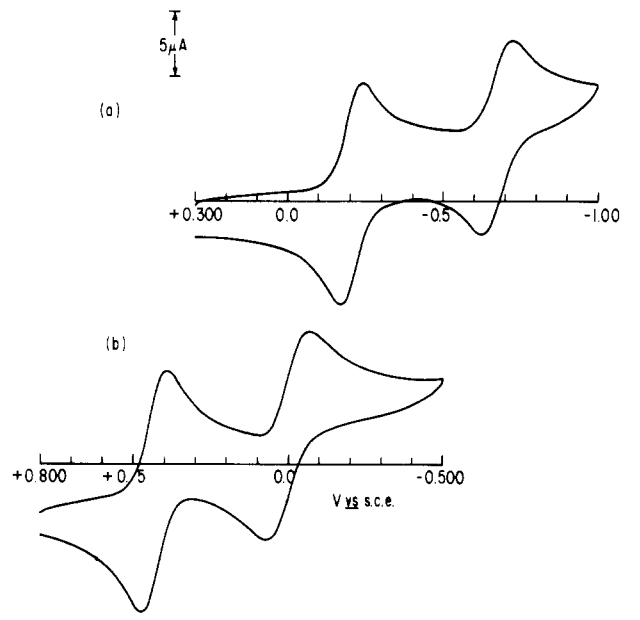

Figure 7. (a) Cyclic voltammogram of $[Mo_4O_{10}(C_6H_2O_4)_2]^{2-}$; (b) cyclic voltammogram of $[Mo_6O_{15}(C_6O_6)_2]^{3-}$. Sweep rate 250 mV s^{-1} at a platinum electrode in 0.2 M $(Bu_4N)PF_6$ in acetonitrile.

C(3)–C(4) and C(9)–C(10) bonds of the ligands. Furthermore, the C(3)–O(10) and C(4)–C(9) distances (1.21 (1) Å, average) are normal benzoquinone distances for double-bond localization in the carbonyl group. In contrast, the C(10)–C(7) and C(9)–O(8) distances are significantly longer (1.25 (1) Å, average), suggesting these as the protonation site. This observation is consistent with the presence of two C=O stretching frequencies in the infrared at 1650 and 1630 cm^{-1} associated with C(4)–O(9)/C(3)–O(10) and C(10)–O(7)/C(9)–O(8), respectively.

Electrochemical Properties. The polynuclear complexes I, III, and IV were examined by cyclic voltammetry at a platinum-wire electrode in acetonitrile containing 0.2 M $[(C_4H_9)_4N]PF_6$. The complexes were electrochemically active, displaying successive, reversible one-electron processes, as listed in Table XII.

Complex I exhibits two successive one-electron reductions, which meet the criteria for diffusion-controlled reversible processes, as

Table XIII. UV/Visible Parameters for the Various Redox Levels of $[Mo_4O_{10}(C_6H_2O_4)_2]^{n-}$ and $[Mo_6O_{15}(C_6O_6)_2]^{n-}$ (n = 2, 3, 4)

complex	λ_{max}, nm (log ϵ)						
$[Mo_4O_{10}(C_6H_2O_4)_2]^{2-}$	764 (3.3)	575 (3.6)		411 (3.8)	366 (4.2)	305 (4.2)	239 (4.4)
$[Mo_4O_{10}(C_6H_2O_4)_2]^{3-}$	737 (sh)	569 (3.3)	467 (sh)	420 (3.9)		304 (4.2)	239 (4.5)
$[Mo_4O_{10}(C_6H_2O_4)_2]^{4-}$			467 (sh)	436 (3.7)		301 (4.5)	242 (4.4)
$[Mo_6O_{15}(C_6O_6)_2]^{2-}$	719 (3.8)	602 (3.7)	530 (4.2)	469 (sh)		330 (4.3)	239 (4.6)
$[Mo_6O_{15}(C_6O_6)_2]^{3-}$		593 (3.2)		462 (3.2)		320 (4.3)	239 (4.6)
$[Mo_6O_{15}(C_6O_6)_2]^{4-}$				466 (3.2)		345 (4.3)	240 (4.6)

shown in Table XII and Figure 7a. The reduction processes are summarized by

$$[Mo_4O_{10}(C_6H_2O_4)_2]^{2-} \overset{-0.208\ V}{\rightleftharpoons} [Mo_4O_{10}(C_6H_2O_4)_2]^{3-} \overset{-0.677\ V}{\rightleftharpoons} [Mo_4O_{10}(C_6H_2O_4)_2]^{4-}$$

Such successive one-electron processes are characteristic of ligand-based redox, rather than metal-centered processes,[40,41] a feature of the electrochemistry that may be confirmed by EPR studies of the paramagnetic one-electron-reduced species, $[Mo_4O_{10}(C_6H_2O_4)_2]^{3-}$. Cyclic voltammetry and double-potential step experiments suggested that the reduced species $[Mo_4O_{10}(C_6H_2O_4)_2]^{3-}$ is stable for at least 5 min at room temperature, while a frozen solution of $[Mo_4O_{10}(C_6H_2O_4)_2]^{3-}$ is indefinitely stable. Controlled-potential electrolysis of a 5×10^{-2} M solution of I in acetonitrile/0.2 M $(Bu_4N)PF_6$ was carried out at −0.320 V. The solution changed in color during the electrolysis from red to purple, and the current decayed linearly with charged passed, q F mol^{-1}, with 1 F mol^{-1} required to complete the reduction. Examination by cyclic voltammetry of the solution before and after electroreduction showed that quantitative conversion of $[Mo_4O_{10}(C_6H_2O_4)_2]^{2-}$ to the stable trinegative anion $[Mo_4O_{10}(C_6H_2O_4)_2]^{3-}$ had occurred.

At the end of a 1 F mol^{-1} electroreduction at −0.320 V, ESR spectra were recorded at room temperature and at −160 °C. The spectrum is a sharp single line centered at $g = 1.999$, characteristic of an unpaired electron localized on ligand orbitals.

Controlled-potential electrolysis of a solution of $[Mo_4O_{10}(C_6H_2O_4)_2]^{3-}$ at −0.800 V resulted in a color change from purple to light brown, accompanied by a linear decay in current with charge passed. At the end of 1 F mol^{-1} electroreduction at this potential, ESR spectra were again recorded. The solutions and frozen samples of $[Mo_4O_{10}(C_6H_2O_4)_2]^{4-}$ were found to be ESR inactive, implying that the additional electron pairs in the ligand-based electron-acceptor orbital.

The primary reductive processes associated with IV are similar to those of I, two successive reversible one-electron reductions. However, the primary reduction occurs at a more positive potential than that associated with I, implying that the LUMO for IV is stabilized by ca. 0.38 V relative to that of I, an observation consistent with the bathochromic shift in the low-energy transitions of the visible spectra from 764 nm for I to 833 nm for IV. It is also noteworthy that the difference between the peak potential for the first and second reductions for I (ΔE) is ca. 0.47 V, whereas the difference between the same processes in IV is only 0.31 V. The more negative potential of the second electroreduction is a consequence of Coulombic repulsions associated with adding an electron to a reduced negatively charged species and with the energy required to pair electrons in the acceptor orbital. Naively, the larger the volume over which the charge is distributed, the smaller the repulsive term. The relative ease of introducing the second electron for IV may simply reflect the considerably larger volume occupied by two interacting $(C_{12}H_4O_5)$ units, compared to two $(C_6H_2O_4)$ groups.

Attempts to study the electron properties of the electroreduced species $[Mo_4O_{10}(C_{12}H_4O_5)_2]^{3-}$ and $[Mo_4O_{10}(C_{12}H_4O_5)_2]^{4-}$ proved unsuccessful due to the relative insolubility of the parent complex and the short lifetime of dilute solutions of the reduced products.

In contrast to the electrochemical behavior of I and IV, complex III exhibits a reversible one-electron reduction at −0.010 V *and* a reversible one-electron *oxidation* at +0.428 V, as shown in Figure 7b and Table XII. The processes are summarized by

$$[Mo_6O_{15}(C_6O_6)_2]^{2-} \overset{+0.428\ V}{\rightleftharpoons} [Mo_6O_{15}(C_6O_6)_2]^{3-} \overset{-0.010\ V}{\rightleftharpoons} [Mo_6O_{15}(C_6O_6)_2]^{4-}$$

The rest state for complex III is one oxidation state negative of the stable form of I, such that the complexes exhibit the identical redox levels but shifted ca. 0.65 V more positive in potential for III relative to I. Cyclic voltammetry and double-potential step experiments indicated that both the oxidized and reduced forms of III are stable for at least 180 s at room temperature; frozen solutions are indefinitely stable. Controlled-potential electrolysis of III at +0.55 V resulted in a color change from the deep purple of III to red-brown for the oxidized species. The current decayed linearly with charge passed, and 1 F mol^{-1} was required to complete the oxidation. The $[Mo_6O_{15}(C_6O_6)_2]^{2-}$ species was EPR inactive, as anticipated, from removal of one electron from the HOMO of $[Mo_6O_{15}(C_6O_6)_2]^{3-}$. Controlled-potential electrolysis at −0.12 V resulted in a yellow-brown solution after a 1 F mol^{-1} reduction. The reduction product $[Mo_6O_{15}(C_6O_6)_2]^{4-}$ is also ESR silent as a consequence of spin-pairing in the ligand-based orbital.

Although the rest states of I and III differ by one redox level, similar ligand-based processes and electronic effects may be invoked. The reductions associated with (I) populate the LUMO, whereas the corresponding orbital for III is the partially occupied HOMO. The HOMO of III is stabilized relative to the LUMO for I, resulting in more positive potentials for both redox processes:

$$[\text{complex}]^{2-} \rightleftharpoons [\text{complex}]^{3-}$$

$$[\text{complex}]^{3-} \rightleftharpoons [\text{complex}]^{4-}$$

Thus, III is more difficult to oxidize and more easily reduced than the corresponding redox state of I. These differences in the electrochemical characteristics of I and III may reflect the substitution of H groups of the ligands in I with electronegative oxygen substituents in III, which would be expected to stabilize the more negative redox states.

The ΔE's, the differences between potentials for the successive redox states, of I and III are remarkably similar, 0.47 and 0.44 V, respectively. Since ΔE is most likely related to interelectronic repulsion effects, the similar ligand volumes associated with $(C_6H_2O_4)$ and (C_6O_6) should result in no dramatic variation in this parameter.

Changes in the redox states of I and III were monitored by UV/visible spectroscopy, and the results are presented in Table XIII. Both complexes in all three oxidation states exhibit two high-energy transitions in the ultraviolet region 238–345 nm. These are most likely internal ligand-based transitions to π^* orbitals of energy inaccessible in the electrochemical window and hence unaffected by these redox processes. Likewise, the transitions in the ranges 411–436 nm for the various oxidation states of I and 462–469 nm for III would appear to be attributed to the $[Mo_2O_5]^{2+}$ chromophore, which is not directly involved in the redox processes and hence should not be grossly perturbed in the redox chemistry. However, the two transitions observed in the 560–760-nm range for the oxidized forms of I and III are dramatically affected by the redox processes.

One-electron reduction of I shifts the 764- and 575-nm bands to higher energies, 732 and 565 nm, respectively. A transition to the LUMO of I will shift to higher energy as a result of

(40) Vella, P.; Zubieta, J. *J. Inorg. Nucl. Chem.* **1978**, *40*, 613.
(41) Hendrickson, A. R.; Martin, R. L.; Rhode, N. M. *Inorg. Chem.* **1976**, *15*, 2115.

interelectronic repulsions and pairing energy requirements that result upon one-electron reduction of I and partial occupation of this orbital. Further reduction to the $[Mo_4O_{10}(C_6H_2O_4)_2]^{4-}$ state fully occupies this level, and no transitions are observed. Similar features in the 590–720-nm region of III also disappear upon two-electron reduction and may be ascribed to transitions involving the electroactive ligand orbital.

Conclusions. The exploitation of polyoxoanions soluble in organic solents allows the isolation of novel oxomolybdate complexes. The chemistry of oxomolybdates with polyhydroxybenzene and polyhydroxyquinone ligands reflects solvent, counterion, and stoichiometry influences.

The complexes I, III, and IV are structurally similar, with two or three $[Mo_2O_5]^{2+}$ units serving to hold the two semiquinone planes in a parallel staggered orientation with short interplanar distances. A major consequence of the overlap of ligand orbitals is significant charge delocalization, facilitating redox chemistry and resulting in a number of readily accessible redox states.

Acknowledgment. This research was supported by NSF Grant CHE8514634.

Supplementary Material Available: Tables S1, S6, S10, and S15, listing bond lengths for I–IV, Tables S2, S7, S11, and S16, listing bond angles for I–IV, Tables S3, S8, S12, and S17, listing anisotropic temperature factors for I–IV, Tables S4, S13, and S18, listing calculated H atom positions, and Table S20, summarizing the crystal data and data collection methods (13 pages); Tables S5, S9, S14, and S19, listing calculated and observed structure factors (52 pages). Ordering information is given on any current masthead page.

Contribution from the Department of Chemistry, Brandeis University, Waltham, Massachusetts 02254

Kinetics and Mechanism of the Oxidation of Hexacyanoferrate(II) by Bromate[1]

Gyula Rábai[2] and Irving R. Epstein*

Received July 12, 1988

The kinetics of the reaction between $Fe(CN)_6^{4-}$ and BrO_3^- have been studied spectrophotometrically in the pH range 3.6–5.8. A mechanism is proposed in which the active species is $Fe(CN)_5H_2O^{3-}$. The mechanism accounts for the observed complex kinetics, including the dependence on reactant concentrations and the effects of light. Numerical simulations with this mechanism give excellent agreement with the experimental results.

Introduction

A recent paper in this series on the systematic design of chemical oscillators reported the occurrence of high-amplitude (pH = 3 to pH = 7) oscillations in the unbuffered reaction of bromate, sulfite, and hexacyanoferrate(II) in a flow reactor (CSTR).[3] This oscillatory system consists of two overall component reactions. First, in a relatively slow, Landolt type, autocatalytic reaction, sulfite is oxidized by bromate, and hydrogen ions are liberated:

$$3HSO_3^- + BrO_3^- \rightarrow 3SO_4^{2-} + Br^- + 3H^+ \quad (1)$$

The second reaction is the bromate oxidation of ferrocyanide, which consumes hydrogen ions:

$$BrO_3^- + 6Fe(CN)_6^{4-} + 6H^+ \rightarrow Br^- + 6Fe(CN)_6^{3-} + 3H_2O \quad (2)$$

The kinetics of the latter reaction have been studied by Birk and Kozub,[4] and the reaction was found to be partially autocatalytic. Their investigations were carried out at a relatively high acidity ($[H^+]$ = 0.05–0.5 M), and the autocatalytic behavior was attributed to the bromine formed in the reaction

$$BrO_3^- + 5Br^- + 6H^+ \rightarrow 3Br_2 + 3H_2O \quad (3)$$

The bromate–bromide reaction is relatively rapid because of the high acid concentration, and its rate increases with accumulation of bromide ion from step 2. The bromine–hexacyanoferrate(II) reaction has also been shown to be very fast.[4]

If we extrapolate Birk and Kozub's results to the higher pHs of interest in the oscillatory system, the rate of the bromate–hexacyanoferrate(II) reaction becomes independent of pH when pH > 3, and its value is too high to allow oscillation in the BrO_3^-–SO_3^{2-}–$Fe(CN)_6^{4-}$ system.[3] Our preliminary experiments showed that the rate depends on the pH, and its value is not as high as expected from Birk and Kozub's results when pH > 3. Consequently, extrapolation of their rate law to lower acidities is not possible.

No other investigations of this reaction appear in the literature. In order to obtain relevant kinetic data for modeling the oscillatory reaction, it is therefore necessary to study the kinetics of the bromate oxidation of hexacyanoferrate(II) under the conditions in which the oscillations occur. In this paper we report such a kinetic study.

The reducing agent hexacyanoferrate(II) plays a role in many mechanistic investigations but in only a few with other oxyhalogen ions, notably with iodate[5,6] and chlorite.[7] A kinetics study of the oxidation of $Fe(CN)_6^{4-}$ by chlorite has been carried out in buffered aqueous solutions at pH 5–7, with $Fe(CN)_6^{4-}$ in excess. This pH range is very close to the one we used, but we have studied the oxidation of hexacyanoferrate(II) in an excess of oxidant.

Experimental Section

Materials. Chemicals used were, where possible, commercial products. All were used without further purification. Aqueous solutions of hexacyanoferrate(II) ion are stable if kept in the dark or in weak diffuse light under argon. There is only a slow aquation reaction, which leads to an equilibrium between the hexacyanoferrate(II) and pentacyanoaquoferrate(II) complexes. Kinetic runs performed with freshly prepared stock solutions of hexacyanoferrate(II) showed some irreproducibilities. It was therefore necessary to leave these solutions overnight at room temperature, under argon, in the dark before use.

Sodium pentacyanoaquoferrate(II) was prepared from pentacyanonitrosylferrate(II) using Hofmann's method[8] as modified by Asperger et al.[9] The stock solution of pentacyanoaquoferrate(II) was prepared with deoxygenated water and was used within 30 min of preparation. Its concentration was determined by spectrophotometry, after oxidation with bromate. $Fe(CN)_5H_2O^{2-}$ has an absorption maximum[10] at 394 nm with an extinction coefficient of ϵ = 743 M^{-1} cm^{-1}.

Kinetics Experiments. It has long been known that reactions of hexacyanoferrate(II) are affected by light and air–oxygen. For this reason, most of the kinetics runs were done in the absence of air and with min-

(1) Systematic Design of Chemical Oscillators. 47. Part 46: Luo, Y.; Epstein, I. R. *J. Phys. Chem.*, in press.
(2) Permanent address: Institute of Physical Chemistry, Kossuth Lajos University, H-4010 Debrecen, Hungary.
(3) Part 45: Edblom, E. C.; Luo, Y.; Orbán, M.; Kustin, K.; Epstein, I. R. *J. Phys. Chem.*, in press.
(4) Birk, J. P.; Kozub, S. G. *Inorg. Chem.* **1973**, *12*, 2460.
(5) Sulfab, Y.; Elfaki, H. A. *Can. J. Chem.* **1974**, *52*, 2001.
(6) Abdel-Khalek, A. A. *Transition Met. Chem. (Weinheim, Ger.)* **1987**, *11*, 67.
(7) Khan, H. A.; Higginson, W. C. E. *J. Chem. Soc., Dalton Trans.* **1981**, 2537.
(8) Hofmann, K. A. *Justus Liebigs Ann. Chem.* **1900**, *312*, 1.
(9) Asperger, S.; Murati, I.; Pavlovic, D. *J. Chem. Soc. A* **1969**, 2044.
(10) Deford, D. D.; Davidson, A. W. *J. Am. Chem. Soc.* **1951**, *73*, 1469.

0020-1669/89/1328-0732$01.50/0